Noise Characterization for Time Interleaved Photonic Analog to Digital Converters

Zhengtao Jin, Guiling Wu, *Member, IEEE*, Sitong Wang, Min Ding, and Jianping Chen

***Abstract*—We build noise models for analyzing the effect of four main noise terms consisting of the amplitude fluctuation of optical sampling pulse trains, timing jitter of optical sampling pulse trains, quantization and aperture jitter noise of electrical analog to digital converters, and noise in photodiodes on time interleaved photonic analog to digital converters. The analyses indicate that the random processes in the optical sampling pulse train and aperture of electrical analog to digital converters have significant effect on both the unmodulated and modulated components in the sampling results. Both quantization noise of electrical analog to digital converters and noise in photodiodes are unrelated to the optical sampling and can be considered as additive noises. Furthermore, we analyzed digital frequency spectra of different noises after time interleaving. To validate the theoretical model, we conduct the corresponding experiments, indicating the experimental results being consistent with the proposed noise models.**

***Index Terms*—Amplitude fluctuation, aperture jitter, digital time interleaving, noise characterization, photodecection noise, timing jitter, time interleaved photonic analog to digital converters.**

I. Introduction

ANALOG to digital converters (ADCs) build a bridge between the analog signals and the digital signals. However, after several years of rapid development, electrical ADCs (EADCs) have reached the plateau of performance due to the electronic bottlenecks such as electronic jitter. This issue can be effectively mitigated by adopting Photonic ADCs (PADCs). Up to now, PADC has attracted plenty of interest and several schemes have been proposed [1]–[9]. By taking advantage of photonics in ultralow jitter and wideband processing and electronics capability, time interleaved PADCs (TIPADCs) are considered as one of the most practically feasible schemes [5]–[8], [10], [11]. With the proposal of solutions for bandwidth, mismatch, distortion etc., the system performance has been improved [6], [12]–[16]. Besides these issues, noise is another essential limiting factor that has to be taken into account and analyzed as it will significantly degrade the performance of TIPADCs. Few analyses of noise in TIPADCs were proposed. Valley *et al.* have analyzed the effect of the optical sampling pulse train noise on the performance of PADCs [17]. However, the effect of photodetection and quantization, and the noise frequency spectrum characteristics are not taken into account. While Gathman and Buckwalter have noticed the main noise factors in TIPADCs at different optical power levels, the quantitative analysis of noise in TIPADCs is absent [15].

In this paper, we model the noises introduced by random processes in TIPADCs and analyze their spectral characteristics by deriving their expression. The analyzed random processes include amplitude fluctuation and timing jitter of the optical sampling pulse train, quantization and aperture jitter noise of EADCs, and noise in photodiodes (PDs). The analyses illustrate the random processes in the optical sampling pulse train and aperture of EADCs have effect on both the unmodulated and modulated components in the sampling results. The noises in unmodulated components are additive noise and located at the frequency close to the zero frequency. The noises in modulated components are multiplicative noise and located near the frequency of the sampled signal. Quantization noise of EADCs and noise in PDs are unrelated to the optical sampling and are additive noise. Moreover, digital frequency spectra of different noises after digital time interleaving are also analyzed. The theoretical analyses are verified experimentally.

II. Basic Model for TIPADCs

Fig. 1 shows the structure of a general TIPADC with N channels [7], [8], [10], [11]. A mode locked laser (MLL) is used to generate an optical sampling pulse train with a broad spectrum and a repetition period of T_s. Then the optical sampling pulse train is split into N trains with a 1-to-N wavelength demultiplexer. These trains pass through optical delay lines with different length, which introduces incremental delays of T_s/N between them. The trains are then recombined with another multiplexer to produce a time-wavelength interleaved optical sampling pulse train with a repetition period of T_s/N. The input microwave signal is intensity modulated onto the time-wavelength interleaved optical sampling pulse train with a Mach-Zehnder modulator (MZM). Afterward, another WDM device routes the optical sampling pulses with the same wavelength into one channel. In each channel, optical sampling pulses are detected by a PD and converted into electrical pulses. Then each electrical pulse is sampled and quantized by a cascaded EADC, where the clock of the EADC is synchronized with the

Manuscript received May 26, 2019; revised September 19, 2019 and November 6, 2019; accepted November 30, 2019. Date of publication December 4, 2019; date of current version March 17, 2020. This work was supported by the National Natural Science Foundation of China (NSFC) under Grant 61535006 and Grant 61627817. *(Corresponding author: Guiling Wu.)*

The authors are with the State Key Laboratory of Advanced Optical Communication Systems and Networks, Department of Electronic Engineering, Shanghai Jiao Tong University, Shanghai 200240, China (e-mail: bigbigjin@foxmail.com; wuguiling@sjtu.edu.cn; wangst@sjtu.edu.cn; mirandading@foxmail.com; jpchen62@sjtu.edu.cn).

Color versions of one or more of the figures in this article are available online at https://ieeexplore.ieee.org.

Digital Object Identifier 10.1109/JLT.2019.2957481

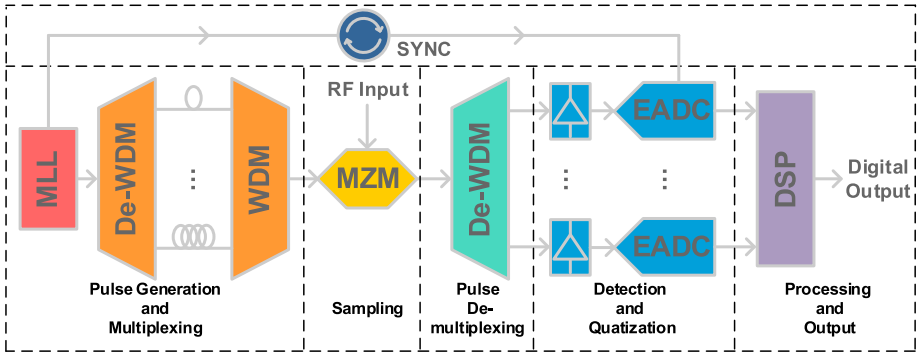

Fig. 1. Scheme of TIPADCs. MLL: Mode Locked Laser; WDM: Wavelength Division Multiplexer; MZM: Mach—Zehnder Modulator; EADC: Electronic analog to digital Converter; DSP: Digital Signal Processing.

repetition rate of the MLL. The final sampling result can be obtained by time interleaving the quantized signals from all the wavelength channels in the digital domain.

For an ideal TIPADC, the intensity of the optical sampling pulse train in the n-th channel can be expressed as

$$p(t) = P_A \sum_{k=-\infty}^{\infty} p_s(t - kT_s - d_p), \tag{1}$$

where $p_s(t)$ is the optical sampling pulse power normalized by the average power, P_A, T_s is the single channel sampling period and $d_p = (n-1)T_s/N$ is the delay of the n-th sub train.

The response of MZM biased at quadrature can be approximated linearly according to the Taylor expansion of the MZM transfer function if the power of the input microwave signal satisfies the small-signal input condition [18]. At the same time, the responsivity of the PD can be also considered as linear under the condition that the pulse energy is far less than the saturation energy [19]. Therefore, the sampling result in the n-th channel can be expressed as

$$v_Q[k] = 0.5\left[1 - h_M(t) * v_I(t)\right] p(t) * h_E(t - d_E)|_{t=kT_s}, \tag{2}$$

where $h_M(t)$ is the small-signal impulse response of MZM, $v_I(t)$ is the microwave signal to be sampled, $h_E(t)$ is the photodetection impulse response including all devices from the PD to the EADC, $d_E = (N-n-1)T_s/N$ is the delay from the MZM to the EADC in the n-th channel, and $*$ denotes the convolution operation.

The ideal sampling result involves two parts: unmodulated component, $v_{Q0}[k]$, and modulated component, $v_{Q1}[k]$:

$$v_Q[k] = v_{Q0}[k] + v_{Q1}[k], \tag{3}$$

where

$$v_{Q0}[k] = 0.5 h_E(t - d_E) * p(t)|_{t=kT_s}, \tag{4}$$

$$v_{Q1}[k] = -0.5 h_E(t - d_E) * [v_I'(t)p(t)]|_{t=kT_s}, \tag{5}$$

$v_I'(t) = v_I(t) * h_M(t)$ denotes the sampled microwave signal modulated on the optical sampling pulse train after filtered by the MZM.

As Eq. (5) indicates, if the sampling rate is too high and/or the photodetection bandwidth is too narrow, adjacent electrical pulses will overlap with each other, resulting in inter symbol interference (ISI)[12]–[14]. The condition without ISI is that the photodetection bandwidth is greater than or equals to half of the single channel sampling rate [12]–[14].

In practice, the performance of the TIPADC, such as effective number of bits (ENOB), will be significantly affected by various random processes in system onto sampling results. The main random processes include amplitude fluctuation, time jitter of optical sampling pulse trains, noise in the photodetection, and noise in EADCs.

Since the noises are generated from different sources, we can take those random processes as independent events [20], [21]. Hence, different kinds of noise can be analyzed independently. Additionally, these random processes can be assumed as wide-sense stationary ones. In the case, the noise can be analyzed with the linear time-invariant operation, and the spectrum of noise can also be obtained [22].

III. Noise Model For TIPADCs

A. Amplitude Fluctuation

Potential sources for amplitude fluctuations of the optical sampling pulse traina mainly involve gain fluctuations and spontaneous emission in MLL [21]. Since the gain fluctuations have long relaxation time, and the power of spontaneous emission is relatively small, typically, the amplitude fluctuations occur at a rate that is slower relative to the optical sampling pulse envelope. Therefore, a set of discrete coherent pulses can be used to describe the optical sampling pulse trains. The intensity of the optical sampling pulse trains in the n-th channel with amplitude fluctuations can be expressed as [20], [21]:

$$p_a(t) = p(t) + p(t)a(t), \tag{6}$$

where $a(t)$ is the zero-mean random function representing relative amplitude fluctuations.

By substituting $p_a(t)$ into Eq. (4), the unmodulated component with amplitude fluctuations can have a form of:

$$\begin{aligned} v_{Q0,a}[k] &= 0.5 h_E(t - d_E) * [p(t) + p(t)a(t)]|_{t=kT_s} \\ &= v_{Q0}[k] + \Delta a_0[k], \end{aligned} \tag{7}$$

where $\Delta a_0[k]$ is the noise in the unmodulated component introduced by the amplitude fluctuations:

$$\begin{aligned}\Delta a_0[k] &= \Delta a_0(t)|_{t=kT_s} \\ &= 0.5h_E(t-d_E) * [p(t)a(t)]|_{t=kT_s}. \end{aligned} \tag{8}$$

From Eq. (7), we can see that $\Delta a_0[k]$ is an additive noise. The Eq. (8) can be rewritten with Eq. (55) in Appendix as

$$\Delta a_0[k] = 0.5\ a(t) * h_a(t)|_{t=kT_s}, \tag{9}$$

where

$$h_a(t) = p(-t)h_E(t-d_E). \tag{10}$$

The analog frequency spectrum of $\Delta a_0(t)$ is

$$\Delta A_0(\Omega) = 0.5A(\Omega)H_a(\Omega), \tag{11}$$

where

$$\begin{cases} H_a(\Omega) = P_A \sum_{m=-\infty}^{\infty} P_s(m\Omega_s)\exp(-im\Omega_s d_p) \\ \qquad \cdot H'_E(\Omega - m\Omega_s) \\ H'_E(\Omega) = H_E(\Omega)\exp(-i\Omega d_E), \end{cases} \tag{12}$$

$\Omega_s = 2\pi/T_s$ is the analog angular frequency and i is the imaginary symbol. In this paper, all the functions denoted by an upper case letter are the Fourier transform of the functions expressed by the corresponding lower case letter.

The corresponding digital frequency spectrum of $\Delta a_0[k]$ can be obtained by using Eq. (11):

$$\Delta A_0(\omega) = \sum_{l=-\infty}^{\infty} \Delta A_0\left(\frac{\omega}{T_s} - \frac{2\pi l}{T_s}\right), \tag{13}$$

where $\omega = \Omega T_s$ is the digital angular frequency.

From Eqs. (9) and (11), we can see that $\Delta a_0[k]$ originates from $a(t)$ transmitting through an equivalent sampling channel where the sampling interval is T_s and the channel impulse response is $h_a(t)$. The equivalent generation procedure of $\Delta a_0[k]$ is shown in Fig. 2(a). The frequency response of the channel, $H_a(\Omega)$, is a weighted sum of the frequency shifted replicas of $H'_E(\Omega)$, where weights are $P_s(m\Omega_s)\exp(-im\Omega_s d_p)$. Fig. 2(b) shows the schematic diagram of $H_a(\Omega)$. In the case of no ISI, the adjacent replicas of $H'_E(\Omega)$ can overlap with each other and form a continuous passband, as shown in Fig. 2(b.1). This will not happen with ISI as shown in Fig. 2(b.2). Thus, there will be ripples on the frequency response, $H_a(\Omega)$, meaning $A(\Omega)$ being frequency selected by $H_a(\Omega)$[12], [16].

For the modulated component, the sampling result is the sum of the signal, $v_{Q1}[k]$, and the sampled noise induced by the amplitude fluctuations, $\Delta a_1[k]$. with amplitude fluctuations and can be obtained by substituting $p_a(t)$ into Eq. (5):

$$\begin{aligned} v_{Q1,a}[k] &= -0.5h_E(t-d_E) * [v'_I(t)p_a(t)]|_{t=kT_s} \\ &= v_{Q1}[k] + \Delta a_1[k], \end{aligned} \tag{14}$$

where $\Delta a_1[k]$ is the noise in the modulated component introduced by the amplitude fluctuations.

$$\begin{aligned}\Delta a_1[k] &= \Delta a_1(t)|_{t=kT_s} \\ &= -0.5h_E(t-d_E) * [v'_I(t)p(t)a(t)]|_{t=kT_s}. \end{aligned} \tag{15}$$

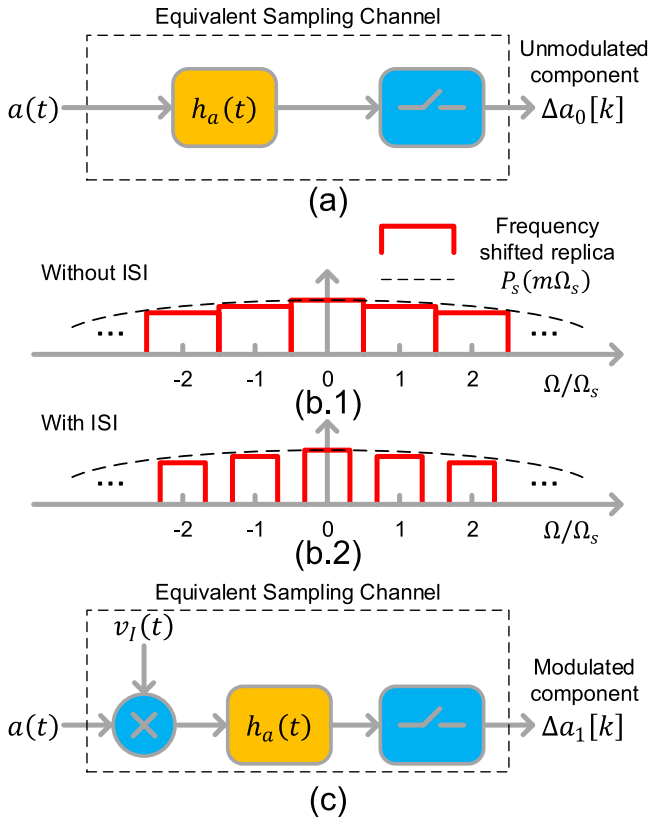

Fig. 2. (a) Equivalent generation procedure of $\Delta a_0[k]$. (b) Schematic diagram of $H_a(\Omega)$. (c) Equivalent generation procedure of $\Delta a_1[k]$.

Here we can see that the noise is multiplicative and depends on the input signal.

With Eq. (55) in Appendix, the expression of the noise can be rewritten as

$$\Delta a_1[k] = -0.5[a(t)v'_I(t)] * h_a(t)|_{t=kT_s}. \tag{16}$$

We can, respectively, obtain the corresponding analog frequency spectrum of $\Delta a_1(t)$ and the digital frequency spectrum of $\Delta a_1[k]$:

$$\Delta A_1(\Omega) = -0.5A(\Omega) * V'_I(\Omega)H_a(\Omega), \tag{17}$$

$$\Delta A_1(\omega) = \sum_{l=-\infty}^{\infty} \Delta A_1\left(\frac{\omega}{T_s} - \frac{2\pi l}{T_s}\right). \tag{18}$$

Equations (16) and (17) indicate $\Delta a_1[k]$ coming from $a(t)$ transmitting through an equivalent sampling channel where $a(t)$ is first multiplied by $v'_I(t)$ and then filtered by $h_a(t)$. The equivalent generation procedure of $\Delta a_1[k]$ is shown in Fig. 2(c).

B. Timing Jitter

The timing jitter in the optical sampling pulse train is mainly from the variation of gain, cavity length, and refractive index, and spontaneous emission in MLL [21]. Compared with the interval of the optical sampling pulse train, the timing jitter is very much short. Therefore, the intensity of the optical sampling pulse train with timing jitter in the n-th channel can be approximated

with a first order Taylor series expansion [20], [21]:

$$p_j(t) = p(t+\delta T) \approx p(t) + T_s j(t)\frac{dp(t)}{dt}, \tag{19}$$

where δT is the small temporal jitter, $j(t)$ is the zero-mean random function, representing the random relative time deviation from the average interval of the optical sampling pulse train, T_s.

For the unmodulated component, the sampling results with timing jitter can be obtained by substituting $p_j(t)$ into Eq. (4):

$$\begin{aligned} v_{Q0,j}[k] &= 0.5h_E(t-d_E) * \left[p(t) + T_s j(t)\frac{dp(t)}{dt}\right]\Big|_{t=kT_s} \\ &= v_{Q0}[k] + \Delta j_0[k], \end{aligned} \tag{20}$$

where $\Delta j_0[k]$ represents the noise in the unmodulated component introduced by the timing jitter. The expression of $\Delta j_0[k]$ is

$$\begin{aligned} \Delta j_0[k] &= \Delta j_0(t)|_{t=kT_s} \\ &= 0.5h_E(t-d_E) * \left[T_s j(t)\frac{dp(t)}{dt}\right]\Big|_{t=kT_s}. \end{aligned} \tag{21}$$

Equation (20) indicates that in the unmodulated component the noise caused by the timing jitter is additive. Since $p(t)$ is a periodic function with a period T_s, its derivative is also a periodic function with the same period. With an assistance of Eq. (55) in Appendix, we can rewrite the expression of $\Delta j_0[k]$ as

$$\Delta j_0[k] = 0.5T_s\ j(t) * h_j(t)|_{t=kT_s}, \tag{22}$$

where

$$h_j(t) = \frac{dp(-t)}{dt} h_E(t-d_E). \tag{23}$$

The corresponding analog frequency spectrum of $\Delta j_0(t)$ and the digital frequency spectrum of $\Delta j_0[k]$ are, respectively,

$$\Delta J_0(\Omega) = 0.5T_s J(\Omega) H_j(\Omega), \tag{24}$$

and

$$\Delta J_0(\omega) = \sum_{l=-\infty}^{\infty} \Delta J_0\left(\frac{\omega}{T_s} - \frac{2\pi l}{T_s}\right), \tag{25}$$

where

$$\begin{aligned} H_j(\Omega) = -iP_A \sum_{m=-\infty}^{\infty} & m\Omega_s P_s(m\Omega_s)\exp(-im\Omega_s d_p) \\ & \cdot H'_E(\Omega - m\Omega_s) \end{aligned} \tag{26}$$

According to Eqs. (22) and (24), $\Delta j_0[k]$ results from $j(t)$ transmitting through an equivalent sampling channel where the sampling interval is T_s and the channel impulse response is $h_j(t)$. Fig. 3(a) shows the equivalent generation procedure of $\Delta j_0[k]$. The frequency response of the channel, $H_j(\Omega)$, is a weighted sum of the frequency shifted replicas of $H'_E(\Omega)$, where the weights are $m\Omega_s P_s(m\Omega_s)\exp(-im\Omega_s d_p)$. The frequency response of the channel, $H_j(\Omega)$, has two kinds of cases: with/without ISI, determined by whether the adjacent replicas of $H'_E(\Omega)$ can overlap or not. Figs. 3(b.1) and (b.2) shows the case with/without ISI, respectively. From Eq. (26), we can see

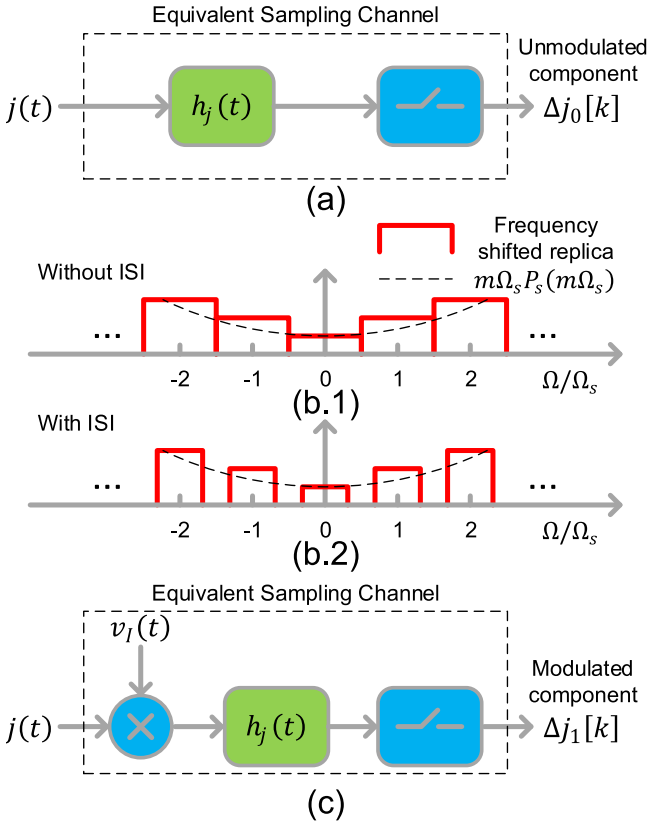

Fig. 3. (a) Equivalent generation procedure of $\Delta j_0[k]$. (b) Schematic diagram of $H_j(\Omega)$. (c) Equivalent generation procedure of $\Delta j_1[k]$.

that the weights, $m\Omega_s P_s(m\Omega_s)\exp(-im\Omega_s d_p)$, increase as the frequency increases. Thus, the product of $H_j(\Omega)$ and $J(\Omega)$, i.e. $\Delta J_0(\Omega)$, becomes larger as the frequency increases in Eq. (24).

For the modulated component, by substituting $p_j(t)$ in Eq. (5), we can obtain the sampling results with timing jitter:

$$\begin{aligned} v_{Q1,j}[k] &= -0.5h_E(t-d_E) * [v'_I(t)p_j(t)]|_{t=kT_s} \\ &= v_{Q1}[k] + \Delta j_1[k], \end{aligned} \tag{27}$$

where $\Delta j_1[k]$ is the noise in the modulated component induced by the timing jitter.

$$\begin{aligned} \Delta j_1[k] &= \Delta j_1(t)|_{t=kT_s} \\ &= -0.5h_E(t-d_E) \\ &\quad * \left[T_s v'_I(t) j(t)\frac{dp(t)}{dt}\right]\Big|_{t=kT_s}. \end{aligned} \tag{28}$$

In the modulated component, the noise induced by the timing jitter is a multiplicative noise. Similarly, the noise can be expressed as

$$\Delta j_1[k] = -0.5T_s\ [v'_I(t)j(t)] * h_j(t)|_{t=kT_s}. \tag{29}$$

With Fourier transform, we can, respectively, have the corresponding analog frequency spectrum of $\Delta j_1(t)$ and the digital frequency spectrum of $\Delta j_0[k]$:

$$\Delta J_1(\Omega) = -0.5T_s V'_I(\Omega) * J(\Omega) H_j(\Omega), \tag{30}$$

and

$$\Delta J_1(\omega) = \sum_{l=-\infty}^{\infty} \Delta J_1\left(\frac{\omega}{T_s} - \frac{2\pi l}{T_s}\right). \tag{31}$$

Equations (29) and (30) indicate that the generation of $\Delta j_1[k]$ can be considered as $j(t)$ transmitting through an equivalent sampling channel where $j(t)$ is firstly frequency shifted by $v_I'(t)$ and then filtered by $h_j(t)$, as shown in Fig. 3(c). As the amplitude of $H_j(\Omega)$ increases with the increase of frequency, the frequency shifted noise item, $V_I'(\Omega) * J(\Omega)$, will be amplified more by $H_j(\Omega)$ at higher frequency, as Fig. 3 (b) shows. Therefore, if the sampled signal have higher frequency components, the noise power introduced by timing jitter will be higher.

C. Noise in EADCs

When EADCs digitize the electrical pulses from PDs, quantization noise and aperture jitter noise are two main kinds of introduced noises. The quantization noise originates from the quantization error during the amplitude discretizing [23]. The quantization error and the amplitude of electrical pulses are strongly correlated. For a typical application, the signals to be sampled by TIPADCs contain complicated frequency components, making the amplitude of electrical pulses random. Therefore, the quantization noise can be assumed as a white noise [23]. The power of the quantization noise is

$$\sigma_Q^2 = \frac{V_{FS}^2}{12 \cdot 4^{N_E}}, \tag{32}$$

where V_{FS} and N_E are the full scale and the ENOB of the EADCs, respectively.

The aperture jitter noise is mainly coming from the sampling clock jitter of EADCs. In TIPADCs, the sampling clock of the EADCs should be synchronized with the repetition rate of the employed MLL so that the every electrical pulse can be quantized. However, the active devices, such as phase locked loops (PLLs) and amplifiers, used for clock synchronization will generate additive noises, resulting in jitters on the sampling clock.

To analyze the effect of the aperture jitter of EADCs, we can equivalently consider the EADC itself is aperture jitter free, while the sampled signals has the timing jitter. In this case, the sampling results can be expressed as

$$\begin{aligned} v_{Q,g}[k] &= \phi(t)|_{t=kT_s+\delta T} \\ &= \phi(t+\delta T)|_{t=kT_s}, \end{aligned} \tag{33}$$

where $\phi(t)$ is the sampled signals.

Considering the jitter is minimal compared to the sampling interval, we can approximate the sampled signals with a first order Taylor series expansion:

$$v_{Q,g}[k] \approx \phi(t) + T_s g(t) \frac{d\phi(t)}{dt}\bigg|_{t=kT_s}, \tag{34}$$

where $g(t)$ is the zero-mean random function of time, representing the relative deviation from the average sampling interval, T_s.

The sampling result is the sum of the sampled signal and the noise induced by the aperture jitter as shown in Eq. (34). In TIPADCs, the sampled electrical signal is the electrical pulse trains:

$$\phi(t) = 0.5 h_E(t - d_E) * \{[1 - v_I'(t)]p(t)\}. \tag{35}$$

By expanding Eq. (35), the additive noise can be also divided into two parts: unmodulated component $\phi_0(t)$, and modulated component $\phi_1(t)$:

$$\begin{cases} \phi(t) = \phi_0(t) + \phi_1(t) \\ \phi_0(t) = 0.5 h_E(t - d_E) * p(t) \\ \phi_1(t) = -0.5 h_E(t - d_E) * [v_I'(t) p(t)] \end{cases}. \tag{36}$$

For the unmodulated component, the noise induced by the aperture jitter can be derived as

$$\begin{aligned} \Delta g_0[k] &= \Delta g_0(t)|_{t=kT_s} \\ &= T_s g(t) \frac{d\phi_0(t)}{dt}\bigg|_{t=kT_s} \\ &= 0.5 T_s g(t) \left[\frac{dh_E(t - d_E)}{dt} * p(t)\right]\bigg|_{t=kT_s}. \end{aligned} \tag{37}$$

With Eq. (55) in Appendix, the expression can be rewritten as

$$\begin{aligned} \Delta g_0[k] &= 0.5 T_s g(t) \left\{\frac{dh_E(t - d_E)}{dt} * [p(t) \cdot 1]\right\}\bigg|_{t=kT_s} \\ &= 0.5 T_s g(t) [h_g(t) * 1]|_{t=kT_s}, \end{aligned} \tag{38}$$

where

$$\begin{cases} h_g(t) = \widehat{h}_E(t - d_E) p(-t), \\ \widehat{h}_E(t) = \frac{d}{dt} h_E(t). \end{cases} \tag{39}$$

In comparison with the photodetection impulse response, the temporal width of the optical sampling pulse is so narrow and can be neglected. Therefore, the temporal power shape of a single optical sampling pulse $p_s(t)$ can be considered as an impulse function $\delta(t)$., and the multi-tap filter $h_g(t)$ can have a from of

$$\begin{aligned} h_g(t) &= \widehat{h}_E(t - d_E) P_A \sum_{q=-\infty}^{\infty} \delta(-t - qT_s - d_p) \\ &= P_A \sum_{q=-\infty}^{\infty} \widehat{h}_E(qT_s - d_p - d_E) \\ &\quad \cdot \delta(t - qT_s - d_p). \end{aligned} \tag{40}$$

where $\widehat{h}_E(qT_s - d_p - d_E)$ is the tap coefficients. When there is no ISI, $h_g(t)$ has only one nonzero coefficient, enabling the filter being a constant gain, $P_A \widehat{h}_E(-d_p - d_E)$. We can observe that the constant gain depend on the derivative of the photodetection impulse response, $\widehat{h}_E(t)$, and the delay from the MZM to the EADC, d_E, which means the noise power is determined by the derivative near the sampling position on electrical pulses of EADCs. More generally, a drastically change of $h_E(t)$ near the sampling position leads to a high value of $h_g(t)$ and high noise power. The corresponding cases include the selection of the rising edge and/or the falling edge of the electrical pulses as the sampling position of EADCs or the narrow temporal width

of the photodetection impulse response. On the contrary, if the value of $h_E(t)$ near the sampling position changes smoothly, the value of $h_g(t)$ will be small and the noise power can be low. For example, we can choose the peak of the $h_E(t)$ as the sampling position or a wide photodetection impulse response temporal width to reduce the noise power.

However, when there is ISI, $h_g(t)$ has multi nonzero coefficients. The gain of the filter is not constant and has frequency selectivity. For the unmodulated component, $1 * h_g(t)$ is a constant, the following equation will be satisfied:

$$\Delta g_0[k] = 0.5T_s P_A \cdot g(t) \sum_{q=-\infty}^{\infty} \widehat{h}_E(qT_s - d_p - d_E)\Big|_{t=kT_s}. \quad (41)$$

Furthermore, the analog frequency spectrum of $\Delta g_0(t)$ and the digital frequency spectrum of $\Delta g_0[k]$ can, respectively, be derived as:

$$\Delta G_0(\Omega) = 0.5T_s G(\Omega) * [2\pi\delta(\Omega) \cdot H_g(\Omega)], \quad (42)$$

and

$$\Delta G_0(\omega) = \sum_{l=-\infty}^{\infty} \Delta G_0\left(\frac{\omega}{T_s} - \frac{2\pi l}{T_s}\right). \quad (43)$$

where

$$H_g(\Omega) = iP_A \sum_{m=-\infty}^{\infty} P_s(m\Omega_s)\exp(-im\Omega_s d_p) \cdot (\Omega - m\Omega_s)H'_E(\Omega - m\Omega_s), \quad (44)$$

As shown in Fig. 4(a), the generation of $\Delta g_0[k]$ can be considered as $g(t)$ transmitting through an equivalent sampling channel where $g(t)$ is multiplied by $1 * h_g(t)$ and sampled with an interval of T_s. The frequency response, $H_g(\Omega)$, is a weighted sum of the frequency shifted replicas of $\Omega H'_E(\Omega)$, where weights are $P_s(m\Omega_s)\exp(-im\Omega_s d_p)$. Fig. 4(b) shows the schematic diagram of $H_g(\Omega)$ in the cases with/without ISI.

For the modulated component, the noise induced by aperture jitter can be derived in the same way:

$$\begin{aligned}\Delta g_1[k] &= \Delta g_1(t)|_{t=kT_s} \\ &= T_s g(t)\frac{d\phi_1(t)}{dt}\Big|_{t=kT_s} \\ &= -0.5T_s g(t)\left\{\widehat{h}_E(t - d_E) * [v'_I(t)p(t)]\right\}\Big|_{t=kT_s}.\end{aligned} \quad (45)$$

With Eq. (55) in Appendix, the expression can be rewritten as

$$\Delta g_1[k] = -0.5T_s g(t)[v'_I(t) * h_g(t)]|_{t=kT_s}. \quad (46)$$

The analog frequency spectrum of $\Delta g_1(t)$ and the digital frequency spectrum of $\Delta g_1[k]$ are

$$\Delta G_1(\Omega) = -0.5T_s G(\Omega) * [V'_I(\Omega) H_g(\Omega)], \quad (47)$$

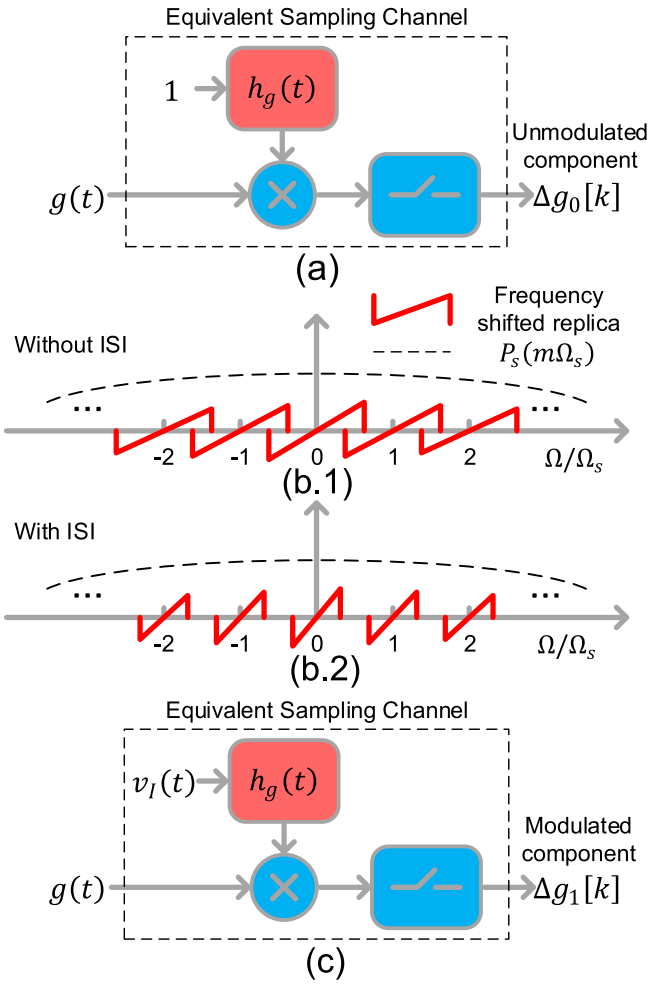

Fig. 4. (a) Equivalent generation procedure of $\Delta g_0[k]$. (b) Schematic diagram of $H_g(\Omega)$. (c) Equivalent generation procedure of $\Delta g_1[k]$.

and

$$\Delta G_1(\omega) = \sum_{l=-\infty}^{\infty} \Delta G_1\left(\frac{\omega}{T_s} - \frac{2\pi l}{T_s}\right). \quad (48)$$

As illustrated in Fig. 4(c), the generation of $\Delta g_1[k]$ with an assistance of Eqs (46) and (47) can be considered as $g(t)$ transmitting through an equivalent sampling channel, where $v'_I(t)$ is first filtered by a filter with an impulse response of $h_g(t)$, and then mixed with $g(t)$. The mixed result is sampled with an interval of T_s. In the case without ISI, the derivative near the sampling position on electrical pulses of EADCs determines the noise power. Similar to the analyses in the unmodulated component in Eq. (40), a drastic change near the sampling position of EADC corresponds to a high noise level. A smooth change near the sampling position of EADC will be useful for suppressing the noise. In the case with ISI, $h_g(t)$ has frequency selectivity.

D. Noise in PDs

The noise introduced by PDs mainly includes thermal noise, shot noise, generation-recombination noise, flicker noise and

so on. Thermal noise is a fluctuating current that results from the random thermal motion of electrons, and its power is proportional to the temperature. The shot noise is related to the discrete nature of electrons and input photons. The power of the shot noise is proportional to the photoelectric current. Generation-recombination noise is mainly coming from random fluctuations in the number of carriers. The flicker noise is the dominant noise in the low frequency range and its spectral density function is proportional to the reciprocal of frequency. All these noises can be considered as additive ones [24].

The spectral distribution of these noises in PD have been investigated widely. For the noise with a bandwidth less than $\Omega_s/2$, its digital frequency spectrum after sampled by EADCs is unchanged from its analog frequency spectrum whereas its digital frequency spectrum after sampled by EADCs is an aliasing result of its analog frequency spectrum in the case of the noise with a bandwidth larger than $\Omega_s/2$.

IV. Digital Time Interleaving

Since microwave signals are sampled alternately by multiple channels in TIPADCs, the final sampling results should be obtained by interleaving the sampling data from the channels.

For an arbitrary time interleaving ADC, the sampling results of the n-th channel can be expressed in the frequency domain as:

$$X_n(\Omega) = \frac{1}{T_s} \sum_{k=-\infty}^{\infty} X_c(\Omega - k\Omega_s)\exp(-i\Omega d_p), \tag{49}$$

where $X_c(\Omega)$ is the frequency spectrum of the sampled signals. We can clearly see that $X_n(\Omega)$ is the sum of frequency shifted replicas of $X_c(\Omega)$, where the frequency shift interval is Ω_s.

The final sampling result of TIPADCs is the sum of all channel sampling results:

$$X_c'(\Omega) = \sum_{n=1}^{N} X_n(\Omega). \tag{50}$$

By substituting $d_p = (n-1)T_s/N$ into Eq. (49), once $X_c(\Omega)$ is the same for all channels, the summation will lead to a remain of the frequency shifted replicas of $X_c(\Omega)$ only at the integral multiples of $N\Omega_s$, while the other frequency shifted replicas of $X_c(\Omega)$ are perfectly canceled. On the other hand, all the frequency shifted replicas of $X_c(\Omega)$ are not canceled, resulting in residual replicas, if $X_c(\Omega)$ is different for different channels. Taking a time interleaving ADC with two channels for example, a schematic diagram of the spectrum cancellation is shown in Fig. 5. In the figure, the red and yellow diagrams represent the spectra of two channels; the blue diagram represents the case that corresponding parts can be perfectly canceled; the green diagram represents the case that they have residual parts.

In TIPADCs, the optical sampling pulse train of each channel is the replicas of the optical sampling pulse train from the MLL. Since the fiber is a passive device, the amplitude fluctuation and timing jitter in the optical sampling pulse train are transmitted to all channels without difference in stable operating TIPADCs. Furthermore, all the EADCs are clocked by the same

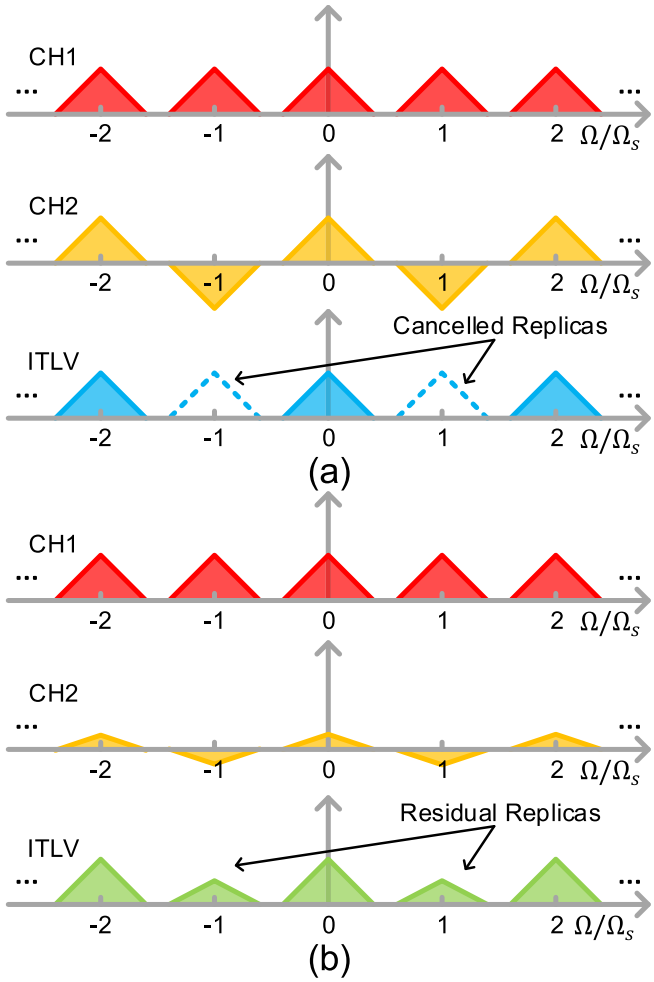

Fig. 5. Schematic diagram of the spectrum cancellation when $X_c(\Omega)$ is the (a) same and (b) different for two channels.

synchronizing signal and sample electrical pulses at the same time, which means the aperture jitter of the EADC in each channel is the same. Thus, for the unmodulated component in the digitized noise caused by the amplitude fluctuation, time jitter, and aperture jitter, $X_c(\Omega)$ is the same. Only the frequency shifted replicas at the integral multiples of $N\Omega_s$ remain and the other replicas are canceled after the digital time interleaving. Additionally, the sampled signal in each channel is identical. For the modulated component of the digitized noise caused by amplitude fluctuation, time jitter, and aperture jitter, $X_c(\Omega)$ is also the same. Therefore, these noises don't have residual parts in the frequency spectrum after digital time interleaving.

Due to the PD in each channel performs independently, the noise in photodetection subjects to independent and identical distribution. Therefore, the EADC in each channel samples different noise signal and obtain different digitized noise, which leads to $X_c(\Omega)$ is different among channels. Consequently, frequency shifted replicas of corresponding noise cannot be canceled during the summation and they will have residual replicas. Different kinds of the noises in photodetection have

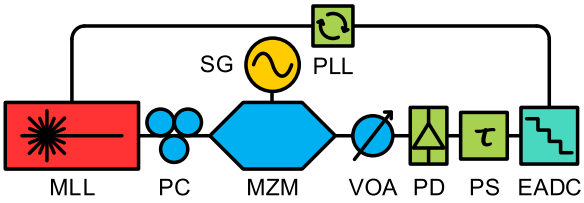

Fig. 6. A single channel TIPADC. MLL: Mode Locked Laser; PC: Polarization Controller; SG: Signal Generator; MZM: Mach—Zehnder Modulator; VOA: Variable Optical Attenuator; PD: Photodiode; PS: Phase Shifter; EADC: Electronic Analog to Digital Converter; PLL: Phase Locked Loop.

different bandwidth. If the noise in photodetection with a bandwidth of less than a half of the sampling rate of a signal channel, the frequency shifted replicas of the noise cannot add up to a constant power spectral density, leaving ripples with a period of Ω_s on the noise spectrum after interleaving. On the contrary, the frequency-shifted replicas of the noise add up to a constant, making the noise spectrum after time interleaving white.

V. Experimental Results

To verify the theoretical models analysed above, a single channel TIPADC is established and shown in Fig. 6. A passive MLL (Precision Photonics, FFL1560) generates the optical sampling pulses at a repetition rate of 36.456 MHz. A microwave signal is produced by a signal generator (Rohde & Schwarz, SMF 100 A) and modulated onto the optical sampling pulse train via a 40 Gbps MZM biased at quadrature. A polarization controller (PC) is used to ensure the polarization of optical sampling pulses is aligned with the z-axis of the used MZM. After demultiplexed, the optical sampling pulse train is attenuated to an average power of $\sim$−l20 dBm with a variable optical attenuator (VOA) to ensure the pulse energy is in the linear region of the responsivity of PDs. Then the optical sampling pulse train is detected by a PD with the bandwidth of 500 MHz. Consequently, electrical pulses from the PD are quantized by an EADC (Keysight, M9703 A) with an analog bandwidth of 1.2 GHz. The EADC is clocked by the MLL via a PLL. A phase shifter (PS) between the PD and the EADC is used to adjust the sampling point of the EADC on the electrical pulses.

Fig. 7 shows the waveform of the sampling results in the time domain, where the frequency of the input microwave signal is 3.6456 MHz. We can observe that the sampling results contains two components: unmodulated component and modulated component. The amplitude of the unmodulated and the modulated component are $\sim$127 mV and $\sim$50 mV, respectively.

The amplitude fluctuation can be estimated with a classic spectrum analysis method [20], [25], [26]. The measurement setup is illustrated in Fig. 8. In the measurement, the used PD has a 5 GHz bandwidth, and two band pass filters (BPFs) with a center frequency of 37 MHz and 3.2 GHz are respectively used for selecting out the fundamental and the 87-th harmonic. The respective phase noise spectrums of the fundamental and the harmonic are measured with a signal source analyzer (Rohde & Schwarz, FSUP).

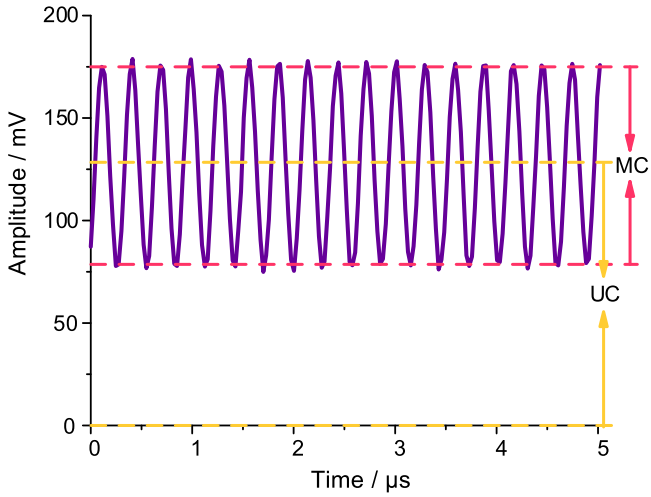

Fig. 7. The waveform of the sampling results in the time domain. UC: Unmodulated Components; MC: Modulated Components.

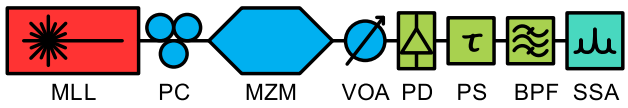

Fig. 8. Amplitude fluctuation measurement setup. MLL: Mode Locked Laser; PC: Polarization Controller; MZM: Mach—Zehnder Modulator; VOA: Variable Optical Attenuator; VDL: Variable Delay Line; PD: Photodiode; BPF: Band Pass Filter; SSA: Signal Source Analyzer.

The phase noise spectra of the fundamental and the 87-th harmonic can be respectively expressed as [20], [25], [26]

$$\begin{cases} P_1(\Omega) = |A(\Omega)|^2 + |J(\Omega)|^2 \\ P_{87}(\Omega) = |A(\Omega)|^2 + |87J(\Omega)|^2. \end{cases} \tag{51}$$

$|A(\Omega)|^2$ can be obtained by solving Eq. (51):

$$|A(\Omega)|^2 = \frac{87^2 P_1(\Omega) - P_{87}(\Omega)}{87^2 - 1}. \tag{52}$$

Fig. 9 shows the measured single band phase noise spectra of the fundamental, the 87-th harmonic, and the calculated single band power spectrum of $|A(\Omega)|^2$. By integrating $|A(\Omega)|^2$, the root mean square (RMS) of the relative amplitude fluctuation of the optical sampling pulse train can be obtained. When the integrating range is from 10 Hz to 1 MHz, the calculated RMS is 0.0754%. After quantization, the corresponding RMS of $\Delta a_0[k]$ and RMS of $\Delta a_1[k]$ are, respectively, $\sim$0.096 mV and $\sim$0.038 mV according to the measured amplitude of the unmodulated component and the modulated component in Fig. 7. The elementary quantization step of the used EADC is $\sim$3.906 mV and the RMS is $\sim$1.128 mV [23]. We can see that the RMSs of $\Delta a_0[k]$ and $\Delta a_1[k]$ are far less than that of the elementary quantization step, illustrating that $\Delta a_0[k]$ and $\Delta a_1[k]$ are very small compared with the quantization noise and considered as neglectable.

The noise in the unmodulated component induced by the timing jitter, $\Delta j_0[k]$, is distributed around zero frequency where

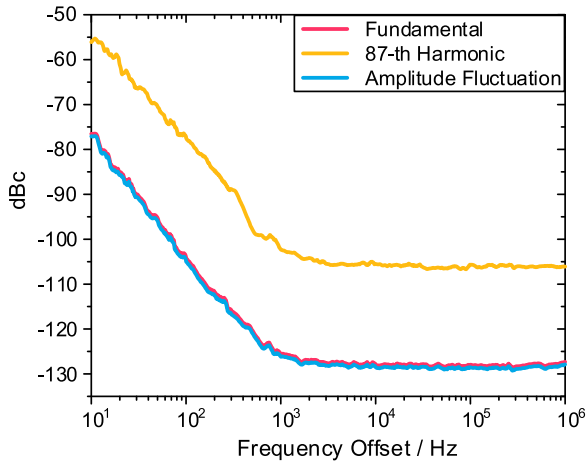

Fig. 9. Single band phase noise spectrum of the fundamental, the 87th harmonic, and the calculated $|A(\Omega)|^2$.

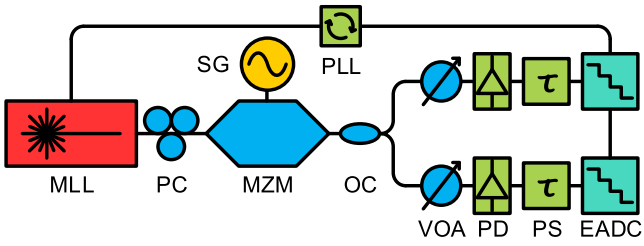

Fig. 10. Measurement setup for testing the noise induced by timing jitter. MLL: Mode Locked Laser; PC: Polarization Controller; SG: Signal Generator; MZM: Mach-Zehnder Modulator; OC: Optical Coupler; VOA: Variable Optical Attenuator; PD: Photodiode; PS: Phase Shifter; EADC: Electronic Analog to Digital Converter; PLL: Phase Locked Loop.

$H_j(\Omega)$ has a small gain according to Eq. (26). Moreover, the power of $j(t)$ is very low for commercial MLLs, resulting in a very low timing jitter. Therefore, the power of $\Delta j_0[k]$ is so small and can be neglected.

A cross correlation method is used to measure the noise in the modulated component induced by the timing jitter, $\Delta j_1[k]$ and avoid the effect of the noise in photodetection. Fig. 10 shows the measurement setup. Here the modulated optical sampling pulse train is divided and fed into two branches via an optical coupler (OC). Each channel contains a VOA, a PD, a PS, and an EADC. In order to measure the $\Delta j_1[k]$, we have to suppress the influence of $\Delta a_1[k]$ and $\Delta g_1[k]$ on the frequency spectrum because all of $J(\Omega)$, $A(\Omega)$ and $G(\Omega)$ are frequency shifted to the frequency of the input microwave signal. According to the discussion above, $\Delta a_1[k]$ can be neglected due to its small magnitude. Furthermore, the sampling position of EADC can be selected at the peak of the electrical pulses to make the derivative of the photodetection impulse response approximated to zero. At this condition, the power of $\Delta g_1[k]$ can be effectively suppressed to zero as indicated in Eq. (40). Among all the analyzed noises, $\Delta j_1[k]$ is the only one related to the input microwave signal frequency. Therefore, the effect of $\Delta j_1[k]$ can be evaluated by increasing the input microwave signal frequency while other noises keep unchanged.

In the cross correlation method, the sampling results of the two branches are

$$\begin{cases} v_{Q,b1}[k] = v'_Q[k] + n_{E,b1}[k] \\ v_{Q,b2}[k] = v'_Q[k] + n_{E,b2}[k] \end{cases}, \tag{53}$$

where $v'_Q[k]$ is the sampling results affected by the noisy optical sampling pulse train, $n_{E,b1}[k]$ and $n_{E,b2}[k]$ are the digitized noise from the PDs.

The cross correlation of the sampling results of the two branches can be written in the frequency domain as [27]

$$\mathcal{F}(v_{Q,b1}[k] \otimes v_{Q,b2}[k]) = \overline{\mathcal{F}}(v_{Q,b1}[k])\mathcal{F}(v_{Q,b2}[k]), \tag{54}$$

where $\otimes$ denotes the cross correlation operation, $\mathcal{F}(\cdot)$ represents the discrete Fourier transform operation and the overbar denotes the complex conjugate.

During the sampling, the optical sampling pulse train is transmitted to both branches without difference. Meanwhile, the PDs and EADCs in both branches produce the noise independently. Thus, $v'_Q[k]$ is the common part between the sampling results in the two branches while $n_{E,b1}[k]$ and $n_{E,b2}[k]$ are the differential part. The differential part between the two channels are uncorrelated and can be canceled after the cross correlation. On the other hand, the common part, including the ideal sampling results and the noise induced by timing jitter, will be dominate [27], [28]. In the experiment, the microwave signals with different frequencies are fed into the TIPADC to examine the relationship between the signal frequency and the noise induced by the timing jitter. The frequencies of the input microwave signals are set to 1.0353504 GHz, 10.0035264 GHz, 20.0289264 GHz, 30.0178704 GHz, and 40.0068144 GHz, respectively. Since the signal frequencies are all beyond the first Nyquist zone of sampling channel, the microwave signals are undersampled and shifted to 14.5824 MHz. To exclude the influence of the nonlinearity frequency response of the MZM as indicated by Eq. (30), the power of the input microwave signal is adjusted to make the magnitude of $v'_I(t)$ constant at different frequencies based on the measured frequency response of the MZM

Fig. 11(a) shows the digital power spectrum of the sampling results after the cross correlation measurement. The frequency is normalized by half of the sampling rate. According to the results, we fit the relative magnitude-frequency response curve shown in Fig. 11(b), where the magnitude of the fitting curve at 1.0353504 GHz is set to 0 dB. We can clearly see that with the increase of the input signal frequency, the noise power also increases since the gain of $H_j(\Omega)$ for $V'_I(\Omega) * J(\Omega)$ is higher at the high frequencies, as Eqs. (26) and (30) indicate.

To demonstrate the effect of the aperture jitter of EADCs on the sampling results, the shape of electrical pulses after photodetection is first measured by an equivalent time sampling method [14] as shown in Fig. 12. In this measurement, no signals are fed into the MZM. Thus, the electrical pulses are all the same. The EADC is clocked by a sinusoidal wave generated by the signal generator. The sinusoidal wave has a small frequency deviation of 2 kHz from the repetition rate of the optical sampling pulse train. The frequency deviation can add a little incremental delay before the next sampling by the EADC to the electrical

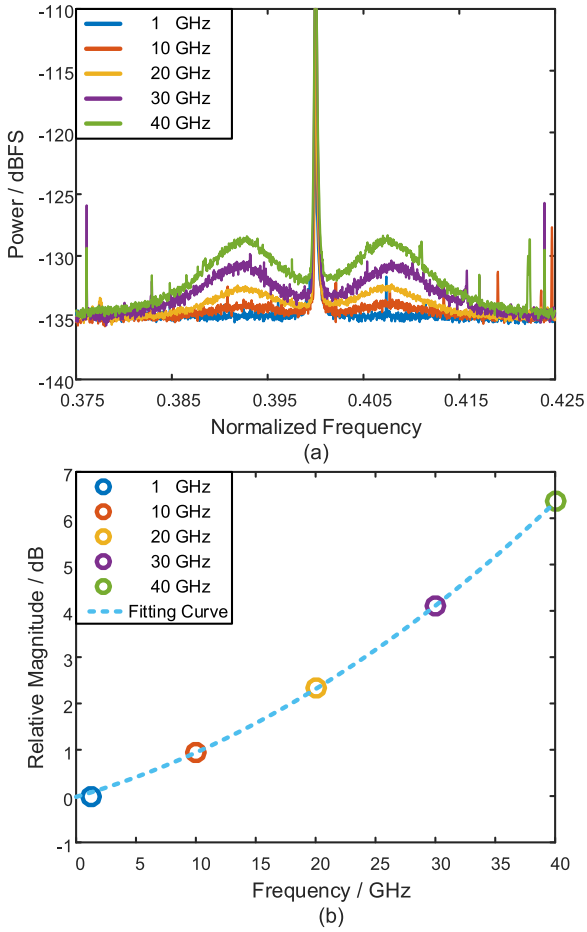

Fig. 11. (a) The measured digital power spectrum based on the cross correlation method. (b) The relative magnitude as a function of frequency.

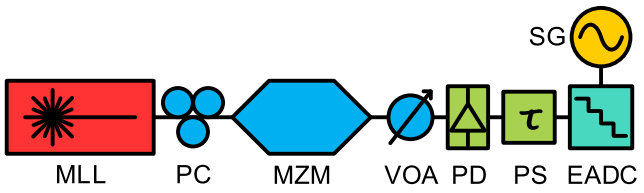

Fig. 12. Photodetection impulse response measurement setup. MLL: Mode Locked Laser; SG: Signal Generator; MZM: Mach-Zehnder Modulator; PD: Photodiode; PS: Phase Shifter; EADC: Electronic Analog to Digital Converter.

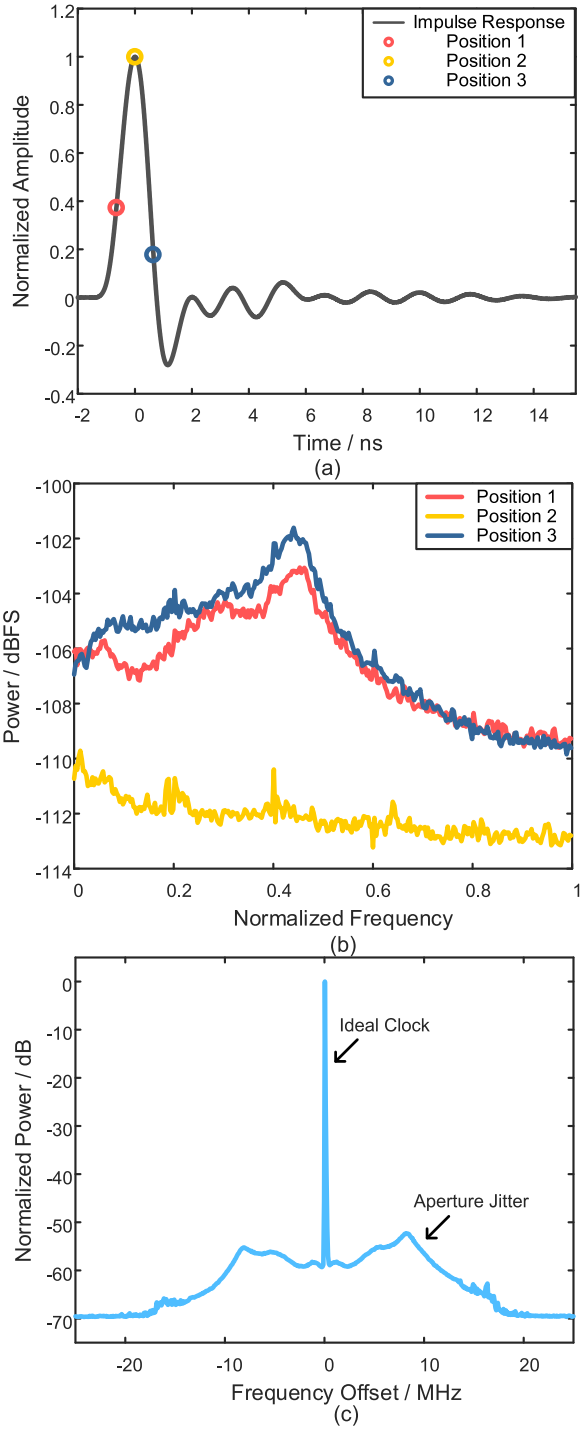

Fig. 13. (a) Measured electrical pulse shape. (b) Digital power spectrums of the noise induced by aperture jitter in the unmodulated component. (c) Spectrum of the EADC sampling clock.

pulse. Because of the periodicity of the electrical pulses, the entire electrical pulse shape can be sampled at a high equivalent sampling rate of ∼664.5 GS/s.

The measurement result of the electrical pulse shape is illustrated in Fig. 13(a). Three different sampling positions of EADC on the electrical pulses are selected, whose absolute values of the derivative are ∼159 V/μs, ∼0 V/μs, and ∼222 V/μs, respectively. Fig. 13(b) show the power spectrums of the sampling results at the three different sampling positions in the unmodulated component. There is no microwave signal fed into the MZM to remove the effect of the modulated component. In this case, the power of the noise induced by the aperture jitter only includes $\Delta g_0[k]$. As we can see, the power of the noise induced by the aperture jitter increases as the absolute value of the derivative increases. When the sampling positions of EADC on the electrical pulses are at the peak of the electrical pulse shape, there is the minimum value of the noise power. Fig. 13(c) shows the spectrum of the EADC sampling clock,

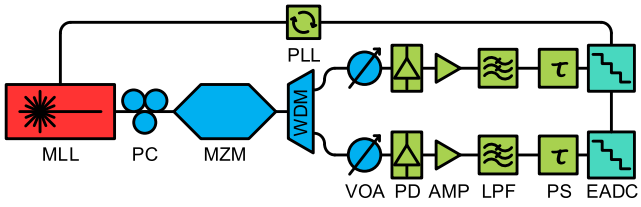

Fig. 14. Experimental setup for measuring the noise induced by timing jitter. MLL: Mode Locked Laser; PC: Polarization Controller; MZM: Mach-Zehnder Modulator; WDM: Wavelength Division Multiplexing; VOA: Variable Optical Attenuator; PD: Photodiode; AMP: Amplifier; LPF: low pass filter; PS: Phase Shifter; EADC: Electronic Analog to Digital Converter; PLL: Phase Locked Loop.

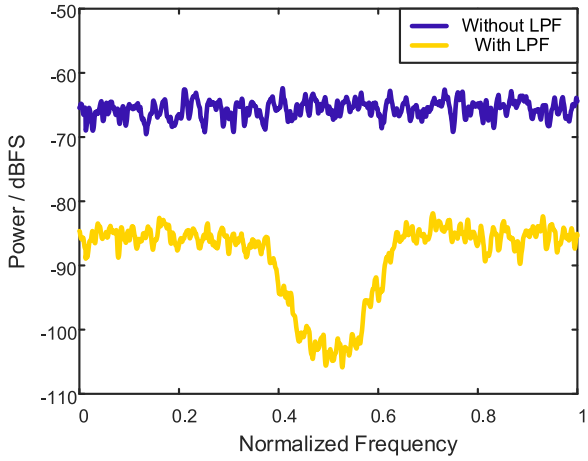

Fig. 15. Digital power spectrums of the noise after time interleaving.

including the ideal clock and aperture jitter measured by the signal source analyzer. By comparing between Figs. 13(b) and (c), we can observe that $\Delta G_0(\Omega)$ at sampling position 1 or 3 has the same power spectral distribution as the noise of the EADC sampling clock, as indicated in Eq. (42). Both of them have a peak at an offset frequency of ∼8 MHz. In Fig. 13(b) the frequency is normalized by half of the sampling rate. The actual frequency at the peak is ∼8 MHz. At sampling position 2, the power of $\Delta G_0(\Omega)$ is very low because of the absolute value of the derivative is approximated to zero. In this case, the effect of $\Delta G_0(\Omega)$ on the power spectral distribution is covered by the noise from the PDs.

When the microwave signal feeds into the MZM, the noise induced by the aperture jitter of the EADC includes both $\Delta g_0[k]$ and $\Delta g_1[k]$. Fig. 7 indicates the magnitude of the modulated component is ∼0.4 times that of the unmodulated component, which means the power of the modulated component is ∼11 dB lower than that of the unmodulated component. By substituting the magnitude of the unmodulated component and the modulated component into Eqs. (42) and (47) respectively, we can find the power density of $\Delta g_1[k]$ is ∼14 dB lower than that of $\Delta g_0[k]$. In this case, the power spectrum of $\Delta g_1[k]$ is buried in that of $\Delta g_0[k]$ in our experiment and has few effect on the total power spectrum of noise induced by the aperture jitter.

To verify the effect of the bandwidth on the photodetection noise in the digital time interleaving results, we design an experimental setup shown in Fig. 14. A WDM is cascaded after the MZM to split the optical sampling pulse train and route into two corresponding channels to stimulate the PD in each channel. Two amplifiers are adopted after PDs to boost the noise generated from PDs. To make the photodetection noise dominant, other noises should be suppressed. Therefore, we select the peak of electrical pulses as the sampling position of the EADCs and no microwave signal feed onto the MZM. Furthermore, an 11 MHz low pass filter (LPF) is used after the amplifier or not to illustrate the cases with different photodetection bandwidth.

Fig. 15(a) and (b) show the measured noise spectra of photodetection with and without LPFs and the corresponding digital noise spectra after time interleaving, where the frequency is normalized by half of the total sampling rate, respectively. As the PDs and EADCs used in the two channels are independent, all the frequency shift replicas cannot be completely canceled after the time interleaving. In the case without LPFs, the bandwidth of the photoreaction is larger than half of the sampling rate of the single channel, making the power density of the noise spectrum after time interleaving becoming a constant. With an assistance of the LPFs, the bandwidth of the photodetection is limited to less than half of the sampling rate of the single channel. It can be seen that digital noise power density is uneven, which is caused by the summation of the frequency shifted noise replicas after the time interleaving has ripples with a period of Ω_s or 0.5 in normalized frequency.

TABLE I
SUMMARY FOR EXPERIMENTAL VERIFICATION

Noise source	Component	Symbol	Frequency response	Verified
Amplitude fluctuation	UC MC	$\Delta a_0[k]$ $\Delta a_1[k]$	$H_a(\Omega)$	- -
Timing jitter	UC MC	$\Delta j_0[k]$ $\Delta j_1[k]$	$H_j(\Omega)$	- ✓
Aperture jitter	UC MC	$\Delta g_0[k]$ $\Delta g_1[k]$	$H_g(\Omega)$	✓ -
Noise in PDs	-	-	-	✓

*UC: Unmodulated Component; MC: Modulated Component.

Table I summarizes the analyzed noises in TIPADCs in the paper. It is worth noting that in our experiments, it is the low amplitude fluctuation of the MLL and the limited quantization resolution of the EADCs that makes the effect of amplitude jitter unable to be observed. The effect of amplitude jitter may become obvious and can be tested in TIPADCs employing MLLs with higher amplitude fluctuation and/or EADCs with higher quantization resolution. The noises induced by timing jitter in the unmodulated component (near zero frequency) and aperture jitter in the modulated component are not observed. The main reasons are as follows respectively: the frequency response of the noise induced by the timing jitter is small near zero frequency according to Eq. (26), and the noises aperture jitter in the modulated component is buried in that in the unmodulated component according to Eqs. (42) and (47).

VI. Conclusion

In this paper, we modeled four main random processes in TIPADCs including the amplitude fluctuation and timing jitter of the optical sampling pulse train, the quantization and the aperture jitter noise of EADCs, and the noise in photodiodes. The spectral characteristics of these noises are analyzed by deriving their expression. Both the unmodulated and modulated components in sampling results can be affected by the random processes in the optical sampling pulse train and aperture of EADCs. The noises in unmodulated components are additive and its frequency around the zero frequency. The noises in modulated components are multiplicative and located at the frequency close to the sampled signal. The quantization noise of EADCs and noise in photodiodes are additive noises uncorrelated to the optical sampling. Moreover, digital frequency spectra of different noises after time interleaving are also analyzed. Experimental measurements on the noises of a TIPADC verify the theoretical results.

Appendix
Equivalent Procedures in Sampling Systems

According to the analysis and proof in [12], [29], for any sampling system, the following equation is satisfied:

$$\begin{aligned} z[k] &= w(t) * [x(t)y(t)]|_{t=kT_s} \\ &= x(t) * [y(-t)w(t)]|_{t=kT_s}, \end{aligned} \tag{55}$$

where $z[k]$ is the sampling results, $w(t)$ and $x(t)$ are arbitrary functions, and $y(t)$ is a function with a period of T_s.

As can be seen from Eq. (55), for the sampling results, the following two procedures are equivalent:

- An arbitrary signal, $x(t)$, is modulated with a periodic signal, $y(t)$, and then sampled synchronously after filtered by $w(t)$;
- An arbitrary signal, $x(t)$ transmits through an equivalent channel and then is sampled synchronously, where the equivalent channel has an impulse response of $y(-t)w(t)$.

In a certain sampling system, both $y(t)$ and $w(t)$ are determined. The analysis of sampling results, $z[k]$, can be simplified by using the two equivalent procedures.

References

[1] G. C. Valley, "Photonic analog-to-digital converters," *Opt. Exp.*, vol. 15, no. 5, pp. 1955–1982, Mar. 2007.

[2] F. Kärtner, A. Khilo, and A. Nejadmalayeri, "Progress in photonic analog-to-digital conversion," in *Proc. Opt. Fiber Commun. Conf./Nat. Fiber Opt. Eng. Conf.*, 2013, Paper OTh3D.5.

[3] F. Coppinger, A. S. Bhushan, and B. Jalali, "Photonic time stretch and its application to analog-to-digital conversion," *IEEE Trans. Microw. Theory Techn.*, vol. 47, no. 7, pp. 1309–1314, Jul. 1999.

[4] A. O. J. Wiberg, "Progress in photonic sampled analog-to-digital conversion," in *Proc. Opt. Fiber Commun. Conf.*, 2015, Paper M2E.1.

[5] H. F. Taylor, "An electrooptic analog-to-digital converter," *Proc. IEEE*, vol. 63, no. 10, pp. 1524–1525, Oct. 1975.

[6] J. C. Twichell and R. Helkey, "Phase-encoded optical sampling for analog-to-digital converters," *IEEE Photon. Technol. Lett.*, vol. 12, no. 9, pp. 1237–1239, Sep. 2000.

[7] T. R. Clark, J. U. Kang, and R. D. Esman, "Performance of a time- and wavelength-interleaved photonic sampler for analog-digital conversion," *IEEE Photon. Technol. Lett.*, vol. 11, no. 9, pp. 1168–1170, Sep. 1999.

[8] P. W. Juodawlkis *et al.*, "Optically sampled analog-to-digital converters," *IEEE Trans. Microw. Theory Techn.*, vol. 49, no. 10, pp. 1840–1853, Oct. 2001.

[9] S. Wang, G. Wu, F. Su, and J. Chen, "Simultaneous microwave photonic analog-to-digital conversion and digital filtering," *IEEE Photon. Technol. Lett.*, vol. 30, no. 4, pp. 343–346, Feb. 2018.

[10] G. Wu, S. Li, X. Li, and J. Chen, "18 wavelengths 83.9gs/s optical sampling clock for photonic a/d converters," *Opt. Exp.*, vol. 18, no. 20, pp. 21 162–21 168, Sep. 2010.

[11] A. Khilo *et al.*, "Photonic ADC: Overcoming the bottleneck of electronic jitter," *Opt. Exp.*, vol. 20, no. 4, pp. 4454–4469, Feb. 2012.

[12] F. Su, G. Wu, L. Ye, R. Liu, X. Xue, and J. Chen, "Effects of the photonic sampling pulse width and the photodetection bandwidth on the channel response of photonic adcs," *Opt. Exp.*, vol. 24, no. 2, pp. 924–934, Jan. 2016.

[13] Z. Jin, G. Wu, C. Wang, and J. Chen, "Inter symbol interference correction based on zero-forcing equalization for time interleaved photonic analog to digital converters," in *Proc. Conf. Lasers Electro Opt.*, 2018, Paper STh3B.5.

[14] Z. Jin, G. Wu, F. Shi, and J. Chen, "Equalization based inter symbol interference mitigation for time-interleaved photonic analog-to-digital converters," *Opt. Exp.*, vol. 26, no. 26, pp. 34 373–34 383, Dec. 2018.

[15] T. D. Gathman and J. F. Buckwalter, "An 8-bit integrate-and-sample receiver for rate-scalable photonic analog-to-digital conversion," *IEEE Trans. Microw. Theory Techn.*, vol. 60, no. 12, pp. 3798–3809, Dec. 2012.

[16] Z. Jin, G. Wu, C. Wang, and J. Chen, "Mismatches analysis based on channel response and an amplitude correction method for time interleaved photonic analog-to-digital converters," *Opt. Exp.*, vol. 26, no. 14, pp. 17 859–17 871, Jul. 2018.

[17] G. C. Valley, J. P. Hurrell, and G. A. Sefler, "Photonic analog-to-digital converters: Fundamental and practical limits," *Proc. SPIE*, vol. 5618, pp. 96–106, 2004.

[18] J. D. McKinney, "Sampled analog links," in *Proc. Avionics, Fiber-Opt. Photon. Technol. Conf.*, Sep. 2010, pp. 47–48.

[19] P. W. Juodawlkis, J. Hargreaves, and J. Twichell, "Impact of photodetector nonlinearities on photonic analog-to-digital converters," in *Proc. Conf. Lasers Electro Opt.*, 2002, Paper CMB7.

[20] D. von der Linde, "Characterization of the noise in continuously operating mode-locked lasers," *Appl. Phys. B*, vol. 39, no. 4, pp. 201–217, Apr. 1986.

[21] D. Eliyahu, R. A. Salvatore, and A. Yariv, "Noise characterization of a pulse train generated by actively mode-locked lasers," *J. Opt. Soc. Amer. B*, vol. 13, no. 7, pp. 1619–1626, Jul. 1996.

[22] U. Mengali and G. Pirani, "Jitter accumulation in pam systems," *IEEE Trans. Commun.*, vol. COMM-28, no. 8, pp. 1172–1183, Aug. 1980.

[23] R. H. Walden, "Analog-to-digital converter survey and analysis," *IEEE J. Sel. Areas Commun.*, vol. 17, no. 4, pp. 539–550, Apr. 1999.

[24] A. Yariv and P. Yeh, *Photonics: Optical Electronics in Modern Communications*. London, U.K.: Oxford Univ. Press, 2006.

[25] M. J. W. Rodwell, D. M. Bloom, and K. J. Weingarten, "Subpicosecond laser timing stabilization," *IEEE J. Quantum Electron.*, vol. 25, no. 4, pp. 817–827, Apr. 1989.

[26] A. Finch, X. Zhu, P. N. Kean, and W. Sibbett, "Noise characterization of mode-locked color-center laser sources," *IEEE J. Quantum Electron.*, vol. 26, no. 6, pp. 1115–1123, Jun. 1990.

[27] J. Breitbarth, "Cross correlation in phase noise analysis," *Microw. J.*, vol. 54, no. 2, pp. 78–85, 2011.

[28] W. F. Walls, "Cross-correlation phase noise measurements," in *Proc. IEEE Freq. Control Symp.*, May 1992, pp. 257–261.

[29] F. Su, G. Wu, and J. Chen, "Photonic analog-to-digital conversion with equivalent analog prefiltering by shaping sampling pulses," *Opt. Lett.*, vol. 41, no. 12, pp. 2779–2782, Jun. 2016.

Zhengtao Jin was born in Henan, China, in 1993. He received the B.S. degree from the University of Electronic Science and Technology of China, Sichuan, China, in 2015. In 2013, he studied at I-Shou University, Taiwan, as an exchange student. He is currently working toward the Ph.D. degree with the State Key Laboratory of Advanced Optical Communication Systems and Networks, Department of Electronic Engineering, Shanghai Jiao Tong University, Shanghai, China. His research interests include microwave photonics and photonic analog-to-digital conversion.

Guiling Wu (M'10) received the B.S. degree from the Harbin Institute of Technology, Harbin, China, in 1995 and the M.S. and Ph.D. degrees from the Huazhong University of Science and Technology, Wuhan, China, in 1998 and 2001, respectively. He is currently a Professor with the State Key Laboratory of Advanced Optical Communication Systems and Networks, Department of Electronic Engineering, Shanghai Jiao Tong University, Shanghai, China. His current research interests include photonic signal processing and transmission.

Sitong Wang was born in Shanghai, China, in 1994. He received the B.S. degree from Shanghai Jiao Tong University, Shanghai, China, in 2016. He is currently working toward the Ph.D. degree with the State Key Laboratory of Advanced Optical Communication Systems and Networks, Department of Electronic Engineering, Shanghai Jiao Tong University, Shanghai. His research interests include microwave photonics, photonic analog-to-digital conversion, and signal processing.

Min Ding was born in Shanghai, China, in 1997. She received the B.S. degree from Shanghai Jiao Tong University, Shanghai, China, in 2019. She is currently working toward the Ph.D. degree with the State Key Laboratory of Advanced Optical Communication Systems and Networks, Department of Electronic Engineering, Shanghai Jiao Tong University. Her research interests include microwave photonics and photonic analog-to-digital conversion.

Jianping Chen received the B.S. degree from Zhejiang University, Hangzhou, China, in 1983 and the M.S. and Ph.D. degrees from Shanghai Jiao Tong University, Shanghai, China, in 1986 and 1992, respectively. He is currently a Professor with the State Key Laboratory of Advanced Optical Communication Systems and Networks, Department of Electronic Engineering, Shanghai Jiao Tong University. His research interests include photonic devices and signal processing, optical networking, and sensing optics. He is also a Principal Scientist of the 973 project in China.